

Controlling the band structure and quench dynamics in one-dimensional optomechanical array driven by a phase modulated laser

Divya Mishra and Parvendra Kumar

*Optics and Photonics Centre, Indian Institute of Technology Delhi, Hauz Khas, New Delhi, 110016
parvendra@opc.iitd.ac.in*

Abstract: We theoretically investigated an array of coupled optomechanical cavities driven by a phase-modulated laser. We show that phase modulation enables the control of band structure and switching of the relative weights of photons and phonons in hybrid eigenmodes. Finally, we show how phase affects the population of hybrid modes and quench dynamics.

1. Introduction

A one-dimensional array of optomechanical resonators provides a tractable platform to investigate and control the interaction between optical and vibrational modes, associated fundamental phenomena, and several practical applications in quantum sensing and information [1-8]. Generally, optomechanical resonators consist of interacting optical and vibrational modes via radiation pressure force. These platforms can be realized with microwave-optomechanical circuits, microdisk resonators, or photonic crystal cavities [9-11]. A variety of controllable degrees of freedom, such as coupling between optical and vibrational modes, resonator geometry, and external control through amplitude or phase modulation of the driving laser, facilitate the observation and realization of many-body phenomena and practical applications [12-14]. Recently, non-reciprocal photon transport has been demonstrated in coupled ring and photonic crystal nanobeam cavities [15, 16]. Moreover, there have been intriguing proposals for exceptional point based sensing and topological photonics with synthesized gauge fields via modulated laser fields [17, 19]. The non-reciprocal flow of phonon was also demonstrated in an optomechanical array (OMA) through the manipulation of band structure [20]. Furthermore, the authors in Ref. [21] investigated quenching dynamics and demonstrated that an OMA can emulate the Su-Schrieffer-Heeger model by controlling a driving laser's power. Here, it may be worthwhile to mention that the quantum quenching pertains to the investigation into the evolution of a many-body system when a parameter in the Hamiltonian undergoes an abrupt alteration during a time frame significantly shorter than any other temporal dynamics [22-25].

In this work, we investigate the effects of the phase-gradient of the driving laser on the quenching dynamics in an array of coupled optomechanical resonators. First, we compute the linearized Hamiltonian of the OMA and then transform it into the Fourier basis for calculating the OMA's eigenmodes and eigenvalues. We demonstrate that the coupling between optical and mechanical modes hybridizes the eigenmodes, resulting in a superposition of photon and phonon modes. We demonstrate that phase-tuning allows us to control the relative weights of photons and phonons in hybrid eigenmodes, thereby significantly influencing the overall band structure. Furthermore, we employ the quantum Langevin equation approach to determine the steady state population of hybrid eigenmodes. A first-order Magnus expansion method is applied to investigate the phase-dependent dynamics of eigenmodes following a sudden change in the optomechanical coupling parameter in the Hamiltonian.

2. Theoretical Model

The model of one-dimensional array of optomechanical resonators is shown in Fig. 1. Here, each site represents a single optomechanical resonator which supports a localized optical (blue circle) and mechanical (red circle) modes. The optomechanical coupling i.e. coupling between optical and mechanical modes is depicted by G . The hopping strengths between the two nearest optical and mechanical modes are represented by J and K , respectively. Additionally, optical mode at each site is driven by a phase modulated laser with site dependent phase, $e^{in\theta}$. This position dependent phase breaks time-reversal symmetry and introduces a position dependent effective coupling between optical and mechanical modes as shown in Fig. 1(b). The Hamiltonian of OMA shown in Fig. 1(a) reads as [1, 20]:

$$H_{sys} = H_s + H_t, \quad (1)$$

$$H_s = \sum_n \omega_c a_n^\dagger a_n + \omega_m b_n^\dagger b_n - G a_n^\dagger a_n (b_n^\dagger + b_n) + \Omega_d \cos(\omega_d + \theta) (a_n^\dagger + a_n), \quad (2a)$$

$$H_t = -J \sum_n (a_n^\dagger a_{n+1} + a_{n+1}^\dagger a_n) - K \sum_n (b_n^\dagger b_{n+1} + b_{n+1}^\dagger b_n) \quad (2b)$$

Here, H_s and H_t represent the Hamiltonians of each sites and tunnelling between them, respectively, G represents a vacuum coupling rate. The bosonic operator a_n (b_n) destroy a photonic (phononic) excitation with energy ω_c (ω_m), Ω_d , ω_d , and θ represent the Rabi frequency, frequency, and phase of the driving laser.

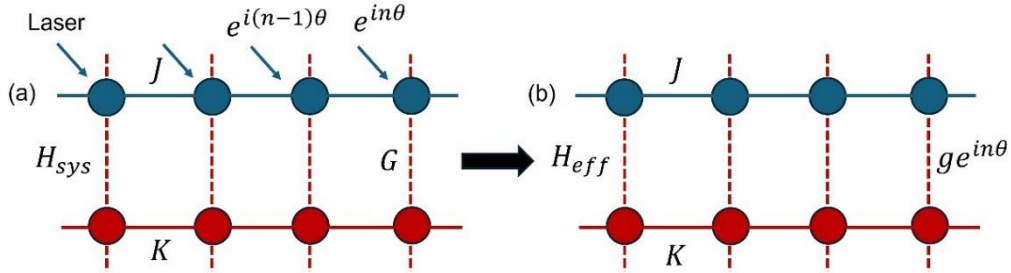


Fig. 1 Schematic of the optomechanical array. (a) Each site consists of a coupled optical mode (blue circle) and a phonon mode (red circle) with coupling strength G . The hopping strengths between nearest neighbour optical and phonon modes are represented by J and K , respectively. The laser driving of optical modes with site dependent phase $e^{in\theta}$ transforms the bare Hamiltonian H_{sys} into an effective Hamiltonian H_{eff} with an enhanced and position dependent optomechanical coupling $g e^{in\theta}$ as shown in (b).

We transform H_{sys} in a frame rotating with angular frequency ω_d together with rotating wave approximation. The linearized effective Hamiltonian reads as [1]:

$$H_{eff} = -\frac{\Delta}{2} \sum_n a_n^\dagger a_n + \frac{\omega_m}{2} \sum_n b_n^\dagger b_n - J \sum_n a_n^\dagger a_{n+1} - K \sum_n b_n^\dagger b_{n+1} - g \sum_n e^{-in\theta} a_n^\dagger b_n + h.c., \quad (3)$$

where $g = G\alpha$ is the optomechanical coupling strength enhanced by factor of α , which is the square root of the average number of photons in the optical mode. This reads as $\alpha = \Omega_d / \left[\left(\Delta + \frac{i\kappa}{2} \right) + 2J \cos\theta + G(\beta + \beta^*) \right]$, $\Delta = (\omega_d - \omega_c)$ and $|\beta|^2$ represents the average number of phonons in the mechanical mode, where $\beta = G|\alpha|^2 / \left[\left(\omega_m - \frac{i\gamma_m}{2} \right) - 2K \right]$, κ and γ_m represent the decay rates of optical and mechanical modes, respectively.

3. Band structure of the optomechanical array

For calculating the band structure of OMA, we transform the Hamiltonian H_{eff} in the Fourier basis by defining the corresponding creation and annihilation operators as $\begin{pmatrix} a_n \\ b_n \end{pmatrix} = \sum_k e^{-inkd} \begin{pmatrix} a_k e^{-in\theta} \\ b_k \end{pmatrix}$, k and d represent the wavenumber and lattice constant, respectively. The Fourier-transformed Hamiltonian H_k is given as:

$$H_k = \begin{pmatrix} -\Delta - 2J \cos(kd + \theta) & -g \\ -g & \omega_m - 2K \cos(kd) \end{pmatrix} \quad (4)$$

The Hamiltonian is an effective approximation for sufficiently large lattices and periodic boundary conditions [20]. The eigen values of H_k are $\omega_k(\pm) = (\Omega - \xi)/2 \pm \sqrt{g^2 + \delta^2}$, $\Omega = \omega_m - 2K \cos(kd)$, $\xi = \Delta + 2J \cos(kd + \theta)$, and $\delta = (\Omega + \xi)/2$. The eigenmodes corresponding to $\omega_k(+)$ and $\omega_k(-)$ are $A_k = \frac{-g}{\sqrt{g^2 + (\delta + \sqrt{g^2 + \delta^2})^2}} a_k + \frac{\delta + \sqrt{g^2 + \delta^2}}{\sqrt{g^2 + (\delta + \sqrt{g^2 + \delta^2})^2}} b_k$ and $B_k =$

$$\frac{-g}{\sqrt{g^2 + (\delta - \sqrt{g^2 + \delta^2})^2}} a_k + \frac{\delta - \sqrt{g^2 + \delta^2}}{\sqrt{g^2 + (\delta - \sqrt{g^2 + \delta^2})^2}} b_k, \text{ respectively. Clearly, both eigen modes consist}$$

superposed optical and mechanical modes and therefore they are termed as hybrid modes. The relative weights of photons and phonons composing the eigenmode A_k are given as $\alpha_A = g^2 / (g^2 + (\delta + \sqrt{g^2 + \delta^2})^2)$ and $\beta_A = (\delta + \sqrt{g^2 + \delta^2})^2 / (g^2 + (\delta + \sqrt{g^2 + \delta^2})^2)$, respectively. Similarly for eigenmode B_k , these are given as $\alpha_B = g^2 / (g^2 + (\delta - \sqrt{g^2 + \delta^2})^2)$ and $\beta_B = (\delta - \sqrt{g^2 + \delta^2})^2 / (g^2 + (\delta - \sqrt{g^2 + \delta^2})^2)$, respectively. Note that the eigen modes can also be written in the compact form as $\begin{pmatrix} A_k \\ B_k \end{pmatrix} = R_k(g) \begin{pmatrix} a_k \\ b_k \end{pmatrix}$, where $R_k(g) = \begin{pmatrix} \alpha_A & \beta_A \\ \alpha_B & \beta_B \end{pmatrix}$.

In Fig. 2, we show how the energy gap between the hybrid eigen modes depend on the normalized wavenumber at different values of g and θ . It is clear from Fig. 2 (a) that the energy gap between the two modes is maximum at $kd = 0$, while it vanishes at the two crossings $kd = \pm\pi/2$. However, for $g = 0.1 \text{ GHz}$, the energy gap opens up with avoided crossings at $kd = \pm\pi/2$ in Fig. 2(b). The band structure changes significantly for $\theta \neq 0$ with a few minima and maxima as shown in Figs. 2(c) and 2 (d). Moreover, for $\theta = 0.9\pi$, band gap becomes asymmetric and shifts toward the higher value of ω_k at $kd = 0.55\pi$, while it shifts toward the lower value of ω_k at $kd = -0.45\pi$. It is worthwhile to mention that such asymmetry has been employed for demonstrating the non-reciprocal transport of phonons [20]. Here, we have shown the effect of phase-mediated asymmetry on the quenching dynamics shown in Figs. 6 and 7.

In Fig. 3, we show the relative weight of photons and phonons composing the hybrid eigenmodes, A_k and B_k as a function of normalized wavenumber at two distinct phases, $\theta = 0$ and π . The eigen mode A_k is mostly phononic in the middle, $-\pi/2 < kd < \pi/2$, and outside it is mostly photonic as can be observed in Fig. 3(a). However, the swapping of relative weights of photons and phonons do occur for $\theta = \pi$, specifically, A_k becomes mostly photonic in the middle, $-\pi/2 < kd < \pi/2$, and outside it is mostly phononic. Similarly, the swapping of relative weights happens in eigen mode B_k for $\theta = \pi$ as shown in Fig. 3(c) and 3(d).

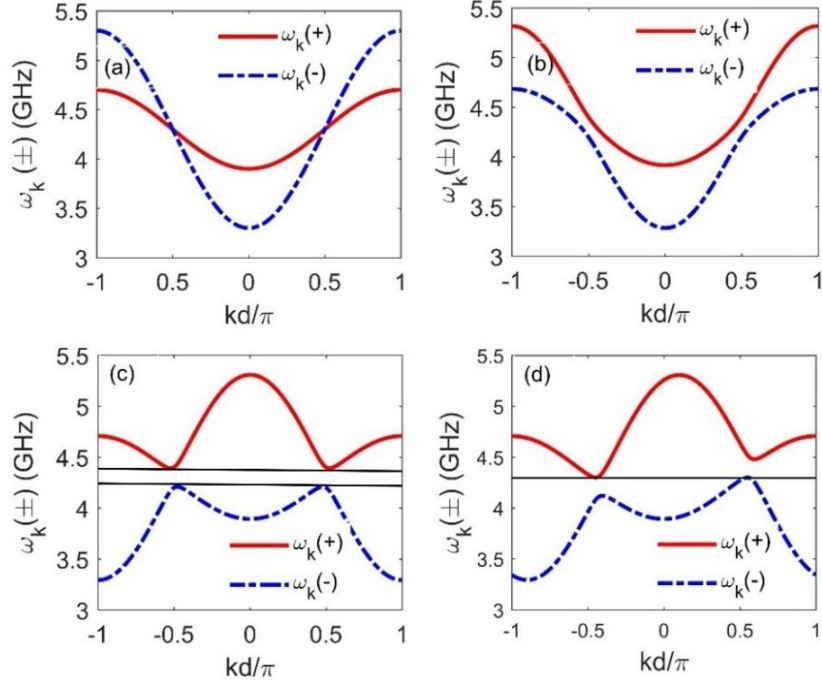


Fig. 2 Energy of the hybrid eigenmodes as a function of normalized wavenumber for detuning $\Delta = -\omega_m$. (a) $g = 0$ and $\theta = 0$, (b) $g = 0.1$ GHz and $\theta = 0$, (c) $g = 0.1$ GHz and $\theta = \pi$, and (d) $g = 0.1$ GHz and $\theta = 0.9\pi$. The value of other simulation parameters is $\omega_m = 4.3$ GHz, $J = 0.5$ GHz, and $K = 0.2$ GHz.

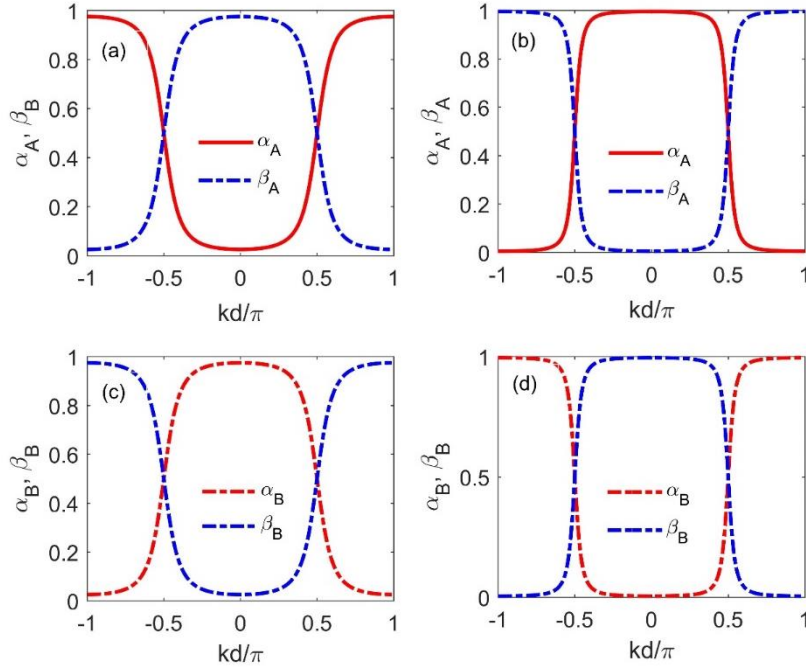


Fig. 3 The relative weights of photons and phonons composing the hybrid eigenmodes. (a) α_A and β_A for $g = 0.1$ GHz and $\theta = 0$, (b) α_A and β_A for $g = 0.1$ GHz and $\theta = \pi$, (c) α_B and β_B for $g = 0.1$ GHz and $\theta = 0$, and (d) α_B and β_B for $g = 0.1$ GHz and $\theta = \pi$. The value of other simulation parameters is same as employed in Fig. 2.

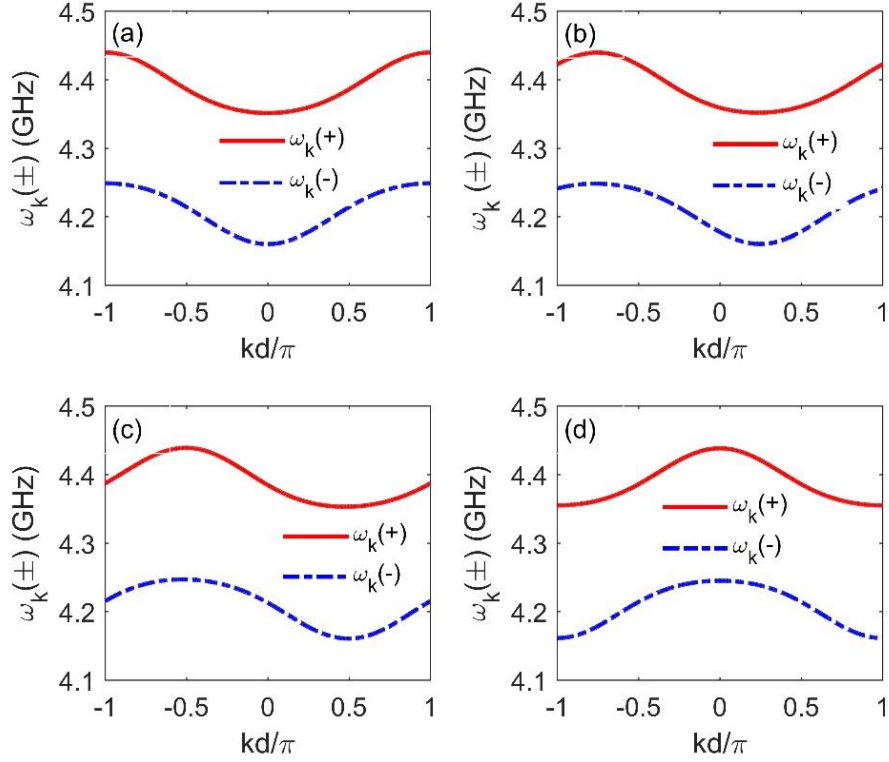


Fig. 4 Energy of the hybrid eigenmodes as a function of normalized wavenumber for detuning $\Delta = -\omega_m$. (a) $\theta = 0$, (b) $\theta = \pi/4$, (c) $\theta = \pi/2$, and (d) $\theta = \pi$. The value of other simulation parameters is $g = 0.086 \text{ GHz}$, $\omega_m = 4.3 \text{ GHz}$, $J = 0.043 \text{ GHz}$, and $K = 0.0013 \text{ GHz}$.

In Fig. 2, we show the band structure for the different values of phase in the parameter regime where $J, K > g$ is satisfied. However, for generality and comparative analysis, we investigate the band structure in the opposite regime as well, i.e. $J, K < g$. It can be observed from Fig. 4 that the energy gap changes as a function of wavenumber and the location of the gap minima also depends on the value of θ . Specifically, the minimum of the gap appears at $kd = \pm\pi/2$ for $\theta = 0$ and π , while it shifts toward $kd = -0.75\pi$ and 0.25π for $\theta = \pi/4$ and toward $kd = 0$ and $\pm\pi$ for $\theta = \pi/2$. For clarity, the variation of energy gap in both cases, $J, K < g$ and $J, K > g$ is shown in Fig. 5(a) and 5(b), respectively. The energy gap minima and maxima are obtained at 0.172 GHz and 0.194 GHz for $\theta = \pi$, as shown in Fig 5(a). Also, it is clear that energy gap maxima values are slightly different for $\theta = 0, \pi/4$, and $\pi/2$. For $J, K > g$, the minimum of the gap also appears at $kd = \pm\pi/2$ for $\theta = 0$ and π . However, it shifts to $kd = -0.87\pi$ and 0.13π for $\theta = \pi/4$, and $kd = -0.13\pi$ and 0.87π for $\theta = \pi/2$. The peak value of energy gap for each chosen θ is substantially different and greater than those are shown in Fig. 5(a). The phase dependent controllability of the minimum energy gap position and peak value of the energy gap manifest themselves in the quench dynamics as shown in Figs. 6 and 7.

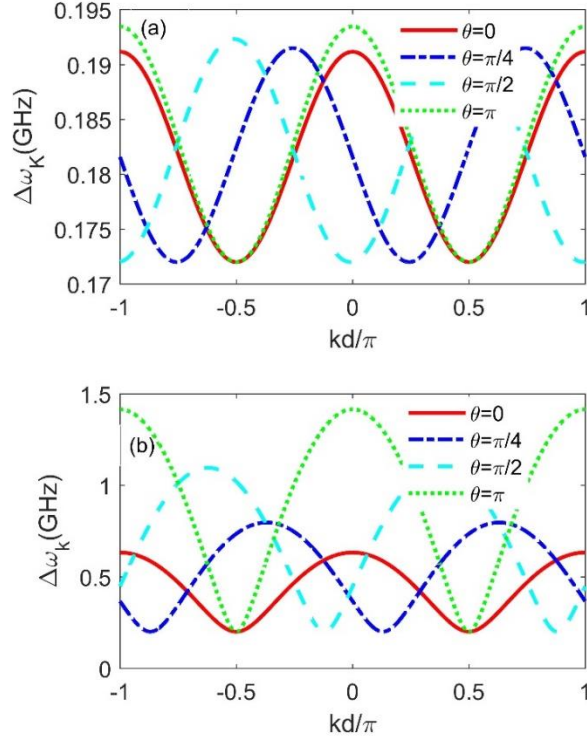


Fig. 5 Energy gap as a function of normalized wavenumber for $\theta = 0$ (solid red line), $\pi/4$ (dashed-dotted blue line), $\pi/2$ (dashed cyan line), and π (dotted green line). (a) $g = 0.086$ GHz, $\omega_m = 4.3$ GHz, $J = 0.043$ GHz, and $K = 0.0013$ GHz, (b) $g = 0.1$ GHz, $\omega_m = 4.3$ GHz, $J = 0.5$ GHz, and $K = 0.2$ GHz.

4. Quenching dynamics in optomechanical array

For investigating the quenching dynamics, we incorporate the phase modulation of driving laser and compute the steady state population of the eigen modes A_k and B_k by following Ref. [21]. The eigen modes population read as: $N_{th}(A_k) = \frac{(1-\alpha_A)\Gamma n_{th}}{\alpha_A \kappa + (1-\alpha_A)\Gamma}$ and $N_{th}(B_k) = \frac{\alpha_A \Gamma n_{th}}{(1-\alpha_A)\kappa + \alpha_A \Gamma}$, respectively, where κ (Γ) and n_{th} represent the decay of optical (mechanical) mode and thermal population in the heat bath. To study the quench dynamics, we replace the coupling g as $g(t) = g\left(1 - \frac{2t}{t_q}\right)$ in Eq. (4), where t_q is the quench time and specifies how fast change is applied to the initial Hamiltonian. We compute the dynamics of eigen modes following a change in Hamiltonian as given below:

$$\begin{pmatrix} A_k(g(t), t) \\ B_k(g(t), t) \end{pmatrix} = R_k(g(t)) S_k(g(t)) \begin{pmatrix} a_k \\ b_k \end{pmatrix} \quad (5)$$

$$\begin{pmatrix} A_k(g(t), t) \\ B_k(g(t), t) \end{pmatrix} = R_k(g(t)) S_k(g(t)) R_k^{-1}(g(0)) \begin{pmatrix} A_k \\ B_k \end{pmatrix}, \quad (6)$$

where time propagator $S_k(g(t))$ gives the evolution of the original modes a_k and b_k as $\begin{pmatrix} a_k(g(t)) \\ b_k(g(t)) \end{pmatrix} = S_k(g(t)) \begin{pmatrix} a_k \\ b_k \end{pmatrix}$ and $\begin{pmatrix} a_k \\ b_k \end{pmatrix} = R_k^{-1}(g(0)) \begin{pmatrix} A_k \\ B_k \end{pmatrix}$. We employ the first order Magnus expansion method (MEM) together with the equations of motion for $a_k(g(t))$ and $b_k(g(t))$ for computing $S_k(g(t))$ [26]. Following MEM, the time propagator is given as:

$$S_k(g(t)) = \begin{pmatrix} \cos\eta(t) - i\frac{\phi(t)}{\eta(t)}\sin\eta(t) & i\frac{\theta(t)}{\eta(t)}\sin\eta(t) \\ i\frac{\theta^*(t)}{\eta(t)}\sin\eta(t) & \cos\eta(t) - i\frac{\phi(t)}{\eta(t)}\sin\eta(t) \end{pmatrix}, \quad (7)$$

where, $\eta(t) = \sqrt{|\theta(t)|^2 + \phi^2(t)}$, $\theta(t) = \frac{g}{2\delta} \left[i(e^{2i\delta t} - 1) - \frac{2ite^{2i\delta t}}{t_q} + \frac{1}{\delta t_q} (e^{2i\delta t} - 1) \right]$, and $\phi(t) = \frac{g^2}{4t_q\delta^3} \xi + \frac{g^2}{t_q\delta} \zeta + \frac{g^2}{2\delta} \chi$. Here, $\xi = \left[1 - \cos(2\delta t) + \frac{2t}{t_q} \cos(2\delta t) - \frac{1}{t_q\delta} \sin(2\delta t) \right]$, $\zeta = \left[\frac{t^2}{2} - \frac{2t^3}{3t_q} \right]$, and $\chi = \left[t - \frac{t^2}{t_q} - \frac{\sin(2\delta t)}{2\delta} + \frac{1}{t_q\delta} t \sin(2\delta t) + \frac{1}{2t_q\delta^2} \{ \cos(2\delta t) - 1 \} \right]$. We derive the eigen mode population $\langle A_k^\dagger A_k(g(t)) \rangle$ and $\langle B_k^\dagger B_k(g(t)) \rangle$ from Eq. 6 together with Eq. 7 and demonstrate their dynamics in Figs. 6 and 7. It is worthwhile to mention that the nature of evolution depends on the quench time, for $t_q \gg \frac{1}{\Delta\omega_k}$ the evolution would be adiabatic, while for $t_q \ll \frac{1}{\Delta\omega_k}$ it would be nonadiabatic, $\Delta\omega_k$ is the energy gap between two the bands. We define and plot the eigen mode population as: $N(A_k) = \langle A_k^\dagger A_k(g(t)) \rangle / n_{th}$ and $N(B_k) = \langle B_k^\dagger B_k(g(t)) \rangle / n_{th}$. Similarly, the net excitation of eigen modes is defined as $N_q(A_k) = (\langle A_k^\dagger A_k(g(t)) \rangle - N_{th}(A_k)) / n_{th}$ and $N_q(B_k) = (\langle B_k^\dagger B_k(g(t)) \rangle - N_{th}(B_k)) / n_{th}$.

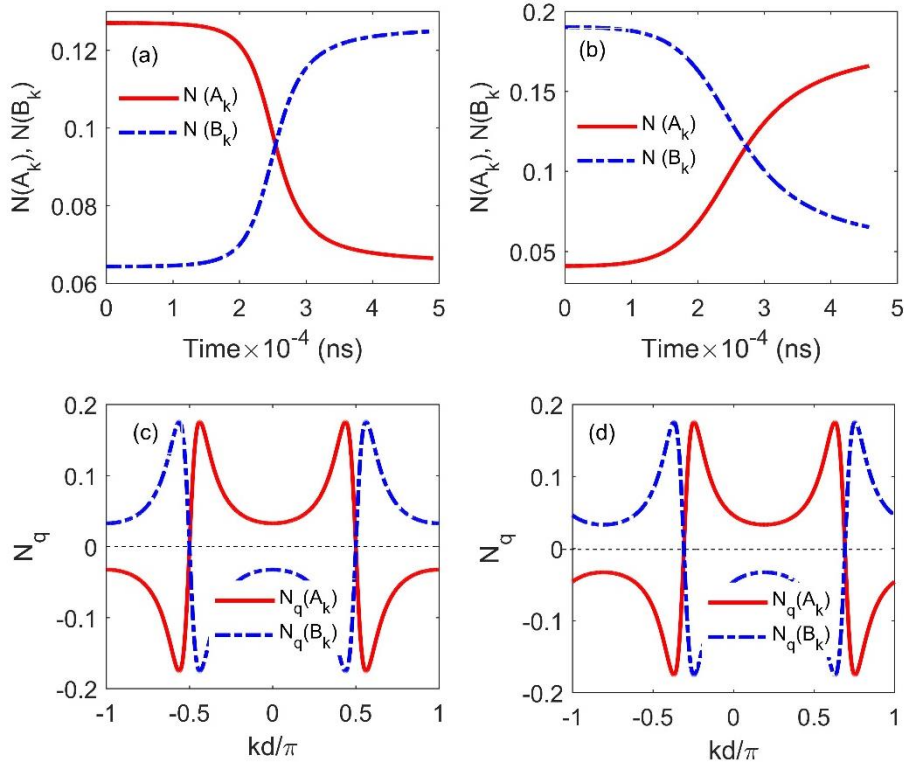


Fig. 6 Quench dynamics for a sudden change of optomechanical coupling from positive to negative: g to $-g$ over a quench time $t_q = \frac{10^{-4}}{\Delta\omega_k}$. Evolution of the eigen modes population through the quench: (a) $kd = 0.48\pi$ and $\theta = 0$, (b) $kd = 0.48\pi$ and $\theta = \pi$. Net excitation in eigen modes through the quench: (c) $\theta = \pi$, and (d) $\theta = 0.8\pi$. The value of other simulation parameters is same as employed in Fig. 2.

It can be observed from Fig. 6(a) the population transition between the two eigen modes take place over the quench and there are the excitations in mode B_k for $\theta = 0$, while in contrast, the excitations occur in mode A_k and its population reach to a maximum value for $\theta = \pi$, as shown in Fig. 6(b). Next in Fig. 6(c), the net excitations in the eigen modes are shown for $\theta = \pi$. These excitations are generated due to the transitions between the eigen modes under nonadiabatic evolution of the system for $t_q \ll \frac{1}{\Delta\omega_k}$. Moreover, they are more pronounced around $kd = \pm 0.5\pi$ because of the smallest energy gap $\Delta\omega_k$ at $kd = \pm \pi/2$, as can be observed in Fig. 2(b). The similar trend of excitations can be observed in Fig 4(d) for $\theta = 0.8\pi$; however, instead of $kd = \pm \pi/2$, the dominant excitations are now shifted to $kd = -0.4\pi$ and 0.6π because of the resulting asymmetry of the band gap as observed in Fig. 2(d).

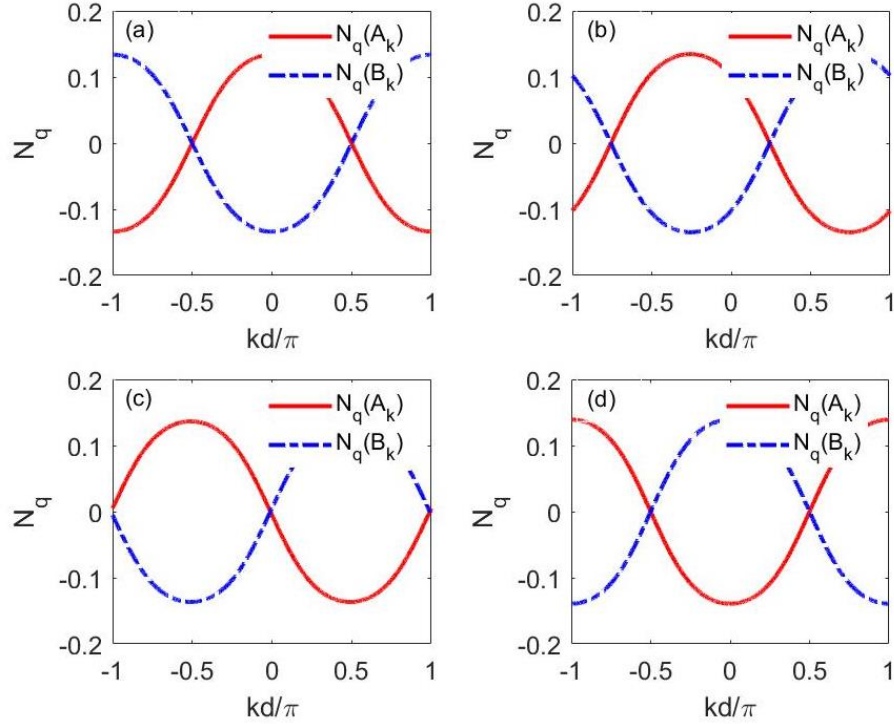


Fig. 7 Net excitation in the eigen modes over a quench time $t_q = \frac{10^{-4}}{\Delta\omega_k}$: (a) $\theta = 0$, (b) $\theta = \pi/4$, (c) $\theta = \pi/2$, and (d) $\theta = \pi$. The value of other simulation parameters is same as used in Fig. 4.

Finally, we show the net excitations in the eigen modes for $J, K > g$. It is clear that for $\theta = 0$, the net excitations are generated around $kd = \pm \pi/2$ due to the minimum energy gap thereat. It may be noted that greater net excitations occur even beyond $kd = \pm \pi/2$ for all values of θ , while in contrast, the excitations get reduced in Figs. 4(c) and 4(d). This occurs because of the greater energy gap as can be comprehended with Fig. 5. For $\theta = \pi/4$, the generation of net excitations are shifted to the location of the minimum energy gap at $kd = -0.87\pi$ and 0.13π . Similarly, in Fig. 7(c) and 7(d), the net excitations are generated at the location of minimum energy gap, which depends on the phase of the driving laser. Therefore, the phase-controlled manipulation of the band structure results in the phase dependent nonadiabatic excitations in the eigen modes.

5. Conclusion

In conclusion, we investigated the effects of phase modulation on the band structure and quench dynamics in an array of optomechanical resonators. We show that due to the optomechanical coupling, the resulting modes are hybrid, composing a superposition of photons and phonons. We demonstrate that manipulating the phase of the driving laser can alter the band structure and the relative weights of photons and phonons. Moreover, we demonstrate that the nonadiabatic evolution of the system through the quench, particularly around the $kd = \pm 0.5\pi$, generates the net excitations, which we can manipulate by altering the laser's phase.

Acknowledgements

P.K. acknowledges support through new faculty seed grant IIT Delhi.

References

- [1] M. Aspelmeyer, T. J. Kippenberg, and F. Marquardt, *Rev. Mod. Phys.* **86**, 1391- 1452 (2014).
- [2] N. Fiaschi, B. Hensen, A. Wallucks, R. Benevides, J. Li, T. P. Mayer Alegre & S. Gröblacher, *Nat. Phot.* **15**, 817–821 (2021).
- [3] S. Pautrel, Z. Denis, J. Bon, A. Borne, and I. Favero, *Phys. Rev. A* **101**, 063820 (2020).
- [4] P. Rakich and F. Marquardt, *New J. Phys.* **20** 045005 (2018).
- [5] D. Vitali, S. Gigan, A. Ferreira, H. R. Bohm, P. Tombesi, A. Guerreiro, V. Vedral, A. Zeilinger, and M. Aspelmeyer, *Phys. Rev. Lett.* **98**, 030405 (2007).
- [6] Deng-Gao Lai, Jie-Qiao Liao, A. Miranowicz, and F. Nori, *Phys. Rev. Lett.* **129**, 063602 (2022).
- [7] B.-y. Zhou, and G.-x. Li, *Phys. Rev. A* **94**, 033809 (2016).
- [8] J. Restrepo, C. Ciuti, and I. Favero, *Phys. Rev. Lett.* **112**, 013601 (2014).
- [9] Safavi-Naeini, A. H., T. P. Mayer Alegre, J. Chan, M. Eichenfield, M. Winger, Q. Lin, J. T. Hill, D. E. Chang, and O. Painter, *Nature (London)* **472**, 69 (2011).
- [10] Safavi-Naeini, A. H., and O. Painter, *Opt. Express* **18**, 14 926 (2010).
- [11] Safavi-Naeini, A. H., and O. Painter, *New J. Phys.* **13**, 013017 (2011).
- [12] M. Schmidt, S. Kessler, V. Peano, O. Painter, and F. Marquardt, *Optica* **2**, 635 (2015).
- [13] J. Vijayan, J. Piotrowski, C. G.-Ballesterro, K. Weber, O. Romero-Isart and L. Novotny, *Nat. Phys.* **20**, 859–864 (2024).
- [14] M. Ludwig and F. Marquardt, *Phys. Rev. Lett.* **111**, 073603 (2013).
- [15] H. Ren, T. Shah, H. Pfeifer, C. Brendel, V. Peano, F. Marquardt and O. Painter, *Nat. Comm.* **13**, 3476 (2022).
- [16] C. Yang, X. Wei, J. Sheng, and H. Wu, *Nat. Comm.* **11**, 4656 (2020).
- [17] J. del Pino, Jesse J. Slim & Ewold Verhagen, *Nat.* **606**, 82-87 (2022).
- [18] H. Jing, Ş. K. Özdemir, H. Lü and F. Nori, *Sci. Rep.* **7**, 3386 (2017).
- [19] P. Djourwe, Y. Pennec, and B. Djafari-Rouhani, *Phys. Rev. Applied* **12**, 024002 (2019).
- [20] A. Seif, W. DeGottardi, K. Esfarjani and M. Hafezi, *Nat. Comm.* **9**, 1207 (2018).
- [21] S. Raeesi, and F. Marquardt, *Phys. Rev. A* **101**, 023814 (2020).
- [22] A. Mitra, *Annu. Rev. Condens. Matter Phys.* **9**, 245 (2018).
- [23] H. Hu and E. Zhao, *Phys. Rev. Lett.* **124**, 160402 (2020).
- [24] A. Polkovnikov, K. Sengupta, A. Silva, and M. Vengalattore, *Rev. Mod. Phys.* **83**, 863 (2011).

- [25] J. Eisert, M. Friesdorf, and C. Gogolin, *Nat. Phys.* 11, 124 (2015).
- [26] T. Begzjav, J. S. Ben-Benjamin, H. Eleuch, R. Nessler, Y. Rostovtsev and G. Shchedrin, *J. Mod. Opt.* 65, 1378–1384 (2018).